6ICEGE 6th International Conference on Earthquake Geotechnical Engineering
1-4 November 2015
Christchurch, New Zealand

New Elastic Spectra, Site Amplification Factors and Aggravation Factors for Complex Subsurface Geometry Towards the Improvement of EC8

K. Pitilakis[1], E. Riga[2], A. Anastasiadis[3], K. Makra[4]

ABSTRACT

Eurocode 8 (EC8) accounts for site effects through the suggestion of appropriate elastic response spectra based on different soil classes and seismic intensity, ignoring, however, complex two-dimensional (2D) site effects related to the existence of subsurface geometry. In the first part of this work, the amplification factors and normalized response spectra currently proposed in EC8 are evaluated using a global database of strong motion records. The estimated amplification factors for classes C and D are significantly higher than the ones proposed in the code. A new soil classification scheme with the associated elastic response spectra is also proposed. In the second part, a numerical 2D seismic response analysis of trapezoidal basins is conducted in order to examine and propose complementary amplification due to basin 2D effects. A comprehensive sensitivity analysis of the different parameters involved, related to the geometry and the soil mechanical properties of the basin, allows to derive conclusions on the nature of the basin effects and to propose simple recommendations for the introduction of basin effects in the seismic design of structures.

Introduction

Based on the results of extended research studies and valuable records after several recent earthquakes like 1989 Loma Prieta, 1994 Northridge and 1995 Kobe, current seismic code provisions have largely accepted the significant role of local site conditions, making however allowance mainly for one-dimensional (1D) site effects (i.e. amplification of ground motion over soft horizontally layered sediments caused by the trapping of seismic waves due to the impedance contrast between the sediments and the underlying bedrock) and ignoring complex two-dimensional (2D) site effects, such as the existence of subsurface geometry or surface topography.

Regarding 1D site effects, their influence is described through appropriate elastic design spectra based on different soil categories and levels of shaking intensity. The main and almost universally adopted parameter for site classification is $V_{s,30}$, i.e. the average shear wave velocity of the upper 30m of the soil profile, calculated from the total time needed for a shear wave to travel these 30m. This parameter, initially introduced by Borcherdt and Glassmoyer (1992), is

[1]Professor, Dept. of Civil Engineering, Aristotle University, Thessaloniki, Greece, kpitilak@civil.auth.gr
[2]Civil Engineer, M.Sc., Dept. of Civil Engineering, Aristotle University, Thessaloniki, Greece, eviriga@civil.auth.gr
[3]Assistant Professor, Dept. of Civil Engineering, Aristotle University, Thessaloniki, Greece, anas@civil.auth.gr
[4]Researcher, Institute of Engineering Seismology and Earthquake Engineering (EPPO), Thessaloniki, Greece, makra@itsak.gr

supposed to provide a quantitative parameterization of the site. In Eurocode 8, hereinafter referred to as EC8 (CEN, 2004), the $V_{s,30}$ parameter is used along with N_{SPT} blow count, plasticity index PI and undrained shear strength C_u to define five soil types (A to E), while two extra special ground types (S1 and S2) are also proposed for special soils (i.e. liquefaction prone site etc). Elastic response spectra are proposed for two different levels of seismic action, Type 1 and Type 2. Type 1 spectra have more energy in long-period motions and are proposed for use in regions having high seismic activity and stronger earthquakes; it is estimated that Type 1 spectra should be used when the earthquakes that contribute to the seismic hazard have a surface wave magnitude M_s greater than 5.5. Type 2 spectra are recommended for $M_s \leq 5.5$, having larger normalized spectral amplitudes at short periods. Ground motion amplification, accounting for local soil and site effects, is expressed through a constant soil factor S, which increases uniformly the normalized elastic response spectra in all periods.

Even if $V_{s,30}$ is not the fundamental parameter to describe site response, it has the "attractive" advantage that it can be obtained easily and at relatively low cost, since the depth of 30m is a typical depth of geotechnical investigations and sampling borings, and has provided engineers with a quantitative parameter for site classification. The main weakness is that the single knowledge of the shear wave velocity profile at the upper 30m cannot quantify properly the effects of the real impedance contrast, which is one of the main causes of soil amplification, as for example in case of shallow (i.e. <15-20m) loose soils on rock or deep soil profiles with variable stiffness and contrast. Hence, the use of $V_{s,30}$ as the basic criterion for site classification in engineering practice, disregarding the soil type, geotechnical criteria and the thickness of soil deposits, combined with the limited number of code site classes, can be misleading in many cases (Pitilakis, 2004). The use of $V_{s,30}$ as a proxy to seismic amplification has been also questioned by several recent works (e.g. Castellaro et al., 2008; Lee and Trifunac, 2010), a summary of which can be found in Pitilakis et al. (2013). In addition, several alternative or supplementary indicators for soil amplification have been suggested, such as depth-to-basement (e.g. Steidl, 2000), average shear wave velocity over depths other than 30m (e.g. Gallipoli and Mucciarelli, 2009; Luzi et al., 2011) or predominant site period/ frequency (e.g. Japan Road Association, 1980; Cadet et al., 2012; Luzi et al., 2011), resulting accordingly in a variety of proposed classification schemes with different parameters defining the different soil classes. Two indicative examples of such classification systems are the ones proposed by Bray and Rodríguez-Marek (1997) and Pitilakis et al. (2004).

Yet, actual soft surface layers are not in general flat but laterally confined in the form of sediment-filled valleys or basins. The finite lateral confinement of the surface layers of such basins introduces additional effects such as generation of surface waves at the edges, which propagate laterally within sediments, resulting to a large enhancement of the sediment amplification (Bard and Bouchon 1980a;b). The constructive interference of basin-induced surface waves with direct shear waves, often referred to as "basin-edge effect", causes amplification in basins, which may be further enhanced by other factors such as focusing, soft-sediment amplification and directivity. The existence of subsurface geometry may also result in 2D resonance patterns (Bard and Bouchon, 1985) and increase of the amplitude and the duration of ground motion.

The shape of the interface between the sediments and the underlying bedrock has been identified as the reason for the spatial variability of observed damages in many cases, such as the 1967

Caracas (Papageorgiou and Kim, 1991), 1985 Michoacán (Sánchez-Sesma et al., 1989), 1988 Armenia (Yegian et al., 1994b; Bielak et al., 1988), 1989 Loma Prieta (Graves, 1993) and 1995 Kobe (Kawase, 1996) earthquakes. Since highly populated areas are often located within sedimentary basins, the prediction of the seismic response of such configurations is of prime interest to geotechnical engineers and engineering seismologists and has therefore been under study for the last five decades. Much of the earliest work on basin response was analytical, providing closed-form exact and approximate solutions to displacement response in time-domain for elastic wave propagation in several simple basin-like configurations (e.g. Trifunac, 1971; Wong and Trifunac, 1974). These closed-form solutions are still widely used to check the accuracy of numerical models. The rapid advances in computing technology over the last decades has facilitated the development of numerical methods for modeling the seismic behaviour of complex subsurface geology in two or three dimensions, as well as the incorporation of non-linear constitutive models for the soil deposits. The main numerical techniques used for modeling the seismic response of sedimentary basins are the Aki-Larner (or discrete wavenumber), finite-difference, finite-element, boundary element, spectral element, weighted residual and ray methods, as well as hybrid methods which combine the advantages of different computational methods. Despite the many numerical and instrumental studies, it has not yet been feasible to incorporate basin effects into seismic building codes, earthquake hazard assessment and risk mitigation policies.

This work has two main goals. The first goal is to examine the adequacy of EC8 normalized response spectra and soil amplification S factors for the existing EC8 soil categories and to propose a new improved soil and site classification system with the accompanying elastic response spectra. The second goal is to explore the sensitivity of 2D seismic response of trapezoidal basins to different parameters, such as geometry of the basin and soil properties, through extensive parametric numerical analyses of the seismic response of homogeneous soil basins and to make some preliminary recommendations to the engineering community for the introduction of basin effects in the seismic design of structures.

Elastic response spectra for EC8

Data selection

In the framework of SHARE project, an extended strong motion database was compiled, by unifying existing national and international databases (Yenier et al., 2010). The database covers earthquakes dating back to 1930s and contains a total of 14193 recordings from 2448 earthquakes recorded at 3708 stations. The soil and site documentation of the stations included in the database is restricted to the $V_{s,30}$ values and site classification according to EC8. Further information on the compilation and characteristics of the database can be found in SHARE (http://www.share-eu.org/). The version of the database used in the present study is v3.1 (March 2010) and contains 13500 records.

For the validation of EC8 elastic response spectra, the analyses were conducted using three different subsets of data with different levels of peak ground acceleration (PGA), all extracted from the main SHARE database. Only recordings corresponding to sites with available classification according to EC8 classification scheme were used. An event magnitude criterion was set, which allowed the use of records with surface wave magnitude $M_s \geq 4$, excluding in this

way small magnitude events. Strong motion recordings with usable spectral period less than 2.5s were also discarded, leading to a dataset of 7161 3-component accelerograms, hereinafter called DS1. In DS1 there are many weak motion records with PGA values less than 20cm/s^2, and only few records with PGA values exceeding 200cm/s^2 (Pitilakis et al., 2012). For this reason, and considering the fact that design spectra should be derived basically from records of strong earthquakes, all the analyses were performed not only for the whole dataset (DS1), but also for two smaller datasets, one with records with PGA greater or equal to 20cm/s^2 (hereafter DS2), and one with records with PGA greater or equal to 150cm/s^2 (hereafter DS3), which may be considered as representative for high seismicity regions.

For the proposal of the new classification system, a subset of the SHARE database was compiled, containing records from sites, which dispose a well-documented soil profile concerning dynamic properties and depth up to the 'seismic' bedrock (V_s>800m/s). This updated database, hereafter called SHARE-AUTH database, contains 3666 strong motion records from 536 stations from Greece, Italy, Turkey, Japan and USA and constitutes a reliable set of empirical measurements for estimation of influence of local site conditions. A more detailed description of the SHARE-AUTH database, as well as a list of all the stations it includes, can be found in Pitilakis et al. (2013). For the 536 stations of the database, new site parameters, not included in the original database, were calculated. These include the thickness of the soil deposits H (i.e. depth to "seismic" bedrock - V_s>800m/s), the time-based average shear wave velocity $V_{s,av}$ of the entire soil deposit and the fundamental period T_0 of the soil deposit. $V_{s,30}$ value for each site was also recalculated.

For the assessment of the elastic response spectra for the soil classes of the new classification system, the same criteria were applied as for the validation of EC8 spectra. As a result, a subset of the SHARE-AUTH database was used (referred to as dataset DS4), consisting of 715 strong motion records with surface wave magnitude M_s≥4, PGA≥20cm/s^2 and usable spectral period T≥2.5s. The number of available strong motion records per EC8 soil class and seismicity type in each one of the four datasets is shown in Table 1. It should be noted that the majority of the records come from sites which are classified as B and C, while few data are actually available for soil classes D and E.

Table 1. Number of strong motion records for each dataset.

Soil Class	**DS1**		**DS2**		**DS3**		**DS4**	
	Type 2	Type 1	Type 2	Type 1	Type 2	Type 1	Type 2	Type 1
A	402	264	105	125	9	23	15	19
B	1508	1896	419	1151	38	214	172	163
C	1133	1775	353	1261	44	219	128	132
D	10	4	3	1	-	-	3	1
E	73	96	33	49	5	7	33	49
Total	3126	4035	913	2587	96	463	351	364

Validation of EC8 normalized elastic response spectra

Datasets DS1, DS2 and DS3 were at first used to validate the spectral shapes proposed in EC8. Datasets DS1 and DS2 were utilized for both seismicity types, while DS3 was considered as

more representative for Type 1 seismicity. The 5% damped spectral values of the two horizontal components were included in the original database. In order to combine the two horizontal components into one single earthquake intensity measure, the geometric mean (GM) of the response spectra for the two orthogonal horizontal components of motion was calculated for each strong motion record. Each GM spectrum was then normalized to the GM PGA of the record. All available records were grouped for the EC8 soil classes and seismicity type. For each soil class and seismicity type the median of these normalized spectra was calculated, along with the 16th and 84th percentiles, which represent the average minus and plus one standard deviation respectively. The normalized empirical response spectra were then compared with the normalized EC8 design spectra. Representative plots for soil classes B and C derived from DS2 dataset for Type 1 seismicity are given in Figure 1.

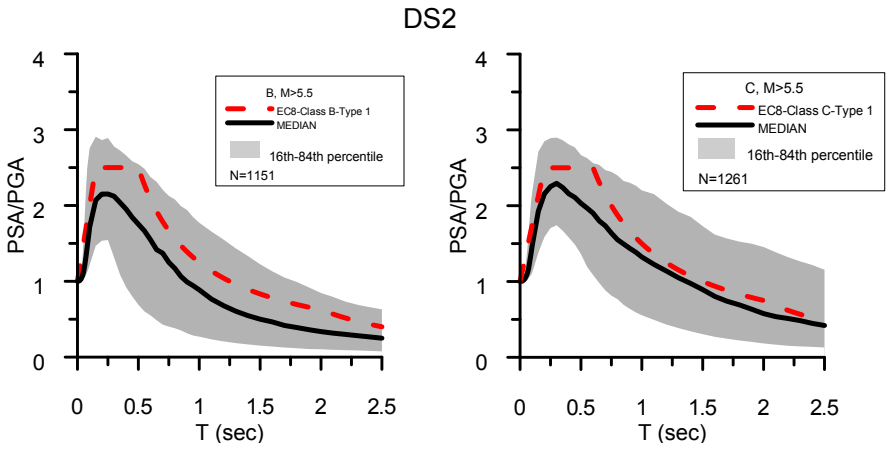

Figure 1. Normalized elastic acceleration EC8 response spectra for Type 1 seismicity against data obtained from DS2 and DS3 datasets for soil class B (left) and soil class C (right).

For soil classes A, B and C the spectral shapes provided by EC8 are generally in good agreement with the derived empirical data for both seismicity types prescribed in EC8. For soil classes D and E the sample of data is not as rich as for the other soil classes and hence the results may not be as convincing as for soil classes A, B and C. However, we found a clear tendency in soil class D spectral shapes to differ substantially from the EC8 shapes. Equally, important differences are found in soil class E where the EC8 spectra seem to be conservative enough for medium and high periods, but probably in short period the plateau should be somehow increased. Another observation is that EC8 elastic spectra do not seem to have been derived based on a common rationale for all soil classes. For example, in some cases (e.g. soil classes A, B and C) EC8 spectra lie between the median and the 84th percentile, while in other cases (e.g. soil class E) EC8 spectra lie closer to or even above the 84th percentile of the empirical normalized spectra. For a more comprehensive presentation of the results the reader is referred to Pitilakis et al. (2012).

Proposal of improved soil amplification factors for EC8 soil classes

For the estimation of improved soil amplification factors for the soil classes of EC8, a logic tree approach was used to account for the epistemic uncertainties (Figure 2). This approach combines two state-of-the-art methods with equal weights. A detailed description of both approaches is

available in Pitilakis et al. (2012). In the first method (Approach 1, Choi and Stewart, 2005) period-dependent amplification factors are calculated using Ground Motion Prediction Equations (GMPEs) for the estimation of reference acceleration spectral values. The amplification factor for ground motion j within site class i, S_{ij}, at spectral period T, is evaluated from the geometric mean of 5% damped acceleration response spectra for the two horizontal components of shaking, GM_{ij}, and the reference ground motion for the site, $(GM_r)_{ij}$, using Equation 1:

$$S_{ij}(T) = GM_{ij} / (GM_r)_{ij} \quad (1)$$

In the above equation, GM_{ij} and $(GM_r)_{ij}$ were computed at the same spectral period, ranging from 0 to 2.5s. The reference motion parameter $(GM_r)_{ij}$ was estimated as the weighted average of the rock predictions of the four GMPEs proposed in SHARE for active shallow crustal regions (Delavaud et al., 2012), since the majority of the SHARE database stations are in active regions. The proposed GMPEs and corresponding weights are shown in Figure 2. The metadata necessary for the implementation of the GMPEs were derived from SHARE strong motion database.

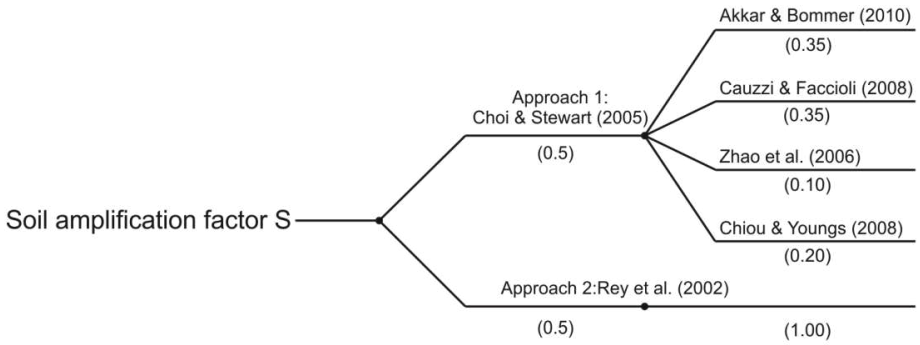

Figure 2. Logic tree used for estimation of soil amplification factors.

In order to estimate, according to Approach 1, a single period-independent amplification factor for each soil class and each seismicity level, similar to the soil factor "S" proposed in EC8, the amplification factors were averaged over a range of periods from T=0 to T=2.0s. Then the derived values were divided by the spectral shape ratio values (SR) in order to isolate the amplification related to the increase of ordinates of soil spectra with respect to rock spectra from the amplification due to the change in shape of PGA-normalized response spectra (Rey et al., 2002).

In the second method (Approach 2, Rey et al., 2002) period-independent amplification factors are calculated for each soil class and for different magnitude intervals (M.I.) of M_s=0.5, with respect to the rock sites of the database using Equation 2:

$$S = (I_{soil} / I_{rock}) \cdot (1 / SR) \quad (2)$$

where SR is the spectral shape ratio, I_{soil} and I_{rock} are the spectrum intensities for soil and rock respectively, originally defined by Housner (1952) for spectral velocities and here adapted for spectral accelerations (Equation 3):

$$I = \int_{0.05}^{2.5} \overline{R \cdot S_a(T)} dt \quad (3)$$

where $\overline{R \cdot S_a(T)}$ denotes the log-average of distance-normalized 5% spectral ordinates $R \cdot S_a(T)$ for each soil class and magnitude interval. I_{soil}/I_{rock} ratios provide a scaling factor for site effect that represents an average amplification globally affecting the whole spectrum (Rey et al., 2002).

Tables 2 and 3 summarize the soil factors obtained for EC8 soil classes with the different approaches and datasets, for Type 2 and Type 1 seismicity, respectively, as well as the weighted average, current EC8 S values and proposed S values. Comparing the determined weighted average S factors with those indicated in EC8 provisions, EC8 factors for class B are in good comparison to the empirical data for both seismicity types, while for soil class C the S factors derived from all datasets are higher compared to EC8. For soil class D the estimated soil factors, which were derived from a limited dataset, are also higher than the EC8 factors for Type 2 seismicity but relatively close to the EC8 factors for Type 1 seismicity. For soil class E, the weighted average soil factors are found quite low for Type 1 seismicity, a result, which is attributed to both the limited data and the averaging process.

Table 2. Soil factors for EC8 soil classes - Type 2 seismicity.

Soil Class	**DS1**			**DS2**			**DS3**			**EC8**	**Proposed**
	Ap.1	Ap.2	W.A.	Ap.1	Ap.2	W.A.	Ap.1	Ap.2	W.A.		
B	0.90	1.55	1.23	1.51	1.37	1.44	-	-	-	1.35	**1.40**
C	1.93	2.54	2.23	2.19	2.12	2.16	-	-	-	1.50	**2.10**
D	3.36	3.07	3.22	2.92	2.00	2.46	-	-	-	1.80	**1.80**[a]
E	0.98	1.79	1.39	1.30	1.96	1.63	-	-	-	1.60	**1.60**[a]

(a) site specific ground response analysis required

Table 3. Soil factors for EC8 soil classes - Type 1 seismicity.

Soil Class	**DS1**			**DS2**			**DS3**			**EC8**	**Proposed**
	Ap.1	Ap.2	W.A.	Ap.1	Ap.2	W.A.	Ap.1	Ap.2	W.A.		
B	1.47	1.34	1.41	1.53	1.08	1.31	1.49	0.94	1.22	1.20	**1.30**
C	2.09	2.24	2.16	2.06	1.46	1.76	1.82	1.15	1.48	1.15	**1.70**
D	1.74	1.42	1.58	1.56	0.92	1.24	-	-		1.35	**1.35**[a]
E	0.91	1.07	0.99	0.97	0.83	0.90	0.93	0.78	0.85	1.40	**1.40**[a]

(a) site specific ground response analysis required

Based on the results derived from this comprehensive study, improved soil factors S are proposed for potential use in an EC8 update, supposing that no further changes are made in the definition of soil classes, seismicity types and the shape of normalized design spectra. The PGA ranges of DS2 and DS3 datasets can be considered as more representative for Type 2 and Type 1 seismicity, respectively. However, since the soil factors obtained from DS2 are more

conservative than the ones obtained from DS3, we decided to keep the soil factors derived from DS2 as more appropriate for both seismicity types. For soil classes D and E, due to the insufficient datasets, it was decided to keep the same S factors as in EC8, knowing however from the few available records that most probably the EC8 amplification factors might be inadequate. Site-specific ground response analyses should be recommended by EC8 for the estimation of soil amplification for soil class D and in some cases for soil class E sites. The proposed soil factors S for EC8 soil classes and seismicity types 1 and 2, are given in Tables 2 and 3, respectively,

New soil classification scheme and elastic response spectra

The classification system proposed herein is an improvement of the scheme proposed by Pitilakis et al. (2004) based on results from theoretical analyses. The proposed improvements were made using exclusively experimental data from the SHARE-AUTH database and concern mainly the limits of values of the parameters describing each soil class. The new improved soil classification system, described in detail in Pitilakis et al. (2013), introduces as primary classification parameters the predominant period of the site (T_0), the depth to bedrock or to a layer with significant impedance contrast and the average shear wave velocity of the entire soil column up to the seismic bedrock ($V_{s,av}$). The secondary parameters are soil type and stratigraphy, as well as the standard penetration test blow count (N_{SPT}), plasticity index (PI) and undrained shear strength (S_u). The proposed classification system is shown in Table 4, where $V_{s,av}$, N_{SPT} and S_u are average values over the whole soil column until the bedrock. This refinement of the proposed by EC8 classification scheme comprises the main factors affecting site response while minimizing the amount of data required for site characterization. In addition, the disaggregation of the effect of soil stratigraphy and/or the soil type on seismic response with different subclasses improves the estimation of ground motion characteristics in many cases and in particular for deep soil profiles, for soft soils and for the case of a thin layer of rather soft soil on very stiff or rock type basement. The new classification system is more precise and practical from a geotechnical engineering point of view and exhibits an improved performance in terms of inter-category error σ_R compared to the classification system of EC8 (Pitilakis et al., 2013).

For the equations describing the proposed normalized response spectra for the soil classes of the new classification system, the general form of the equations proposed by EC8 was adopted, allowing however for a differentiation of spectral amplification parameter β, which in EC8 is constant and equal to 2.5:

$$0 \le T \le T_B : \frac{S_a(T)}{PGA_{rock}} = S \cdot \left[1 + \frac{T}{T_B} \cdot (\beta - 1) \right] \tag{4}$$

$$T_B \le T \le T_C : \frac{S_a(T)}{PGA_{rock}} = S \cdot \beta \tag{5}$$

$$T_C \le T \le T_D : \frac{S_a(T)}{PGA_{rock}} = S \cdot \beta \cdot \frac{T_C}{T} \tag{6}$$

$$T_D \le T : \frac{S_a(T)}{PGA_{rock}} = S \cdot \beta \cdot T_C \cdot \left(\frac{T_D}{T^2} \right) \tag{7}$$

where PGA_{rock} is the design ground acceleration at rock-site conditions, S is the soil amplification factor, T_B and T_C are the limits of the constant spectral acceleration branch, T_D is the value defining the beginning of the constant spectral displacement range of the spectrum and β is the spectral amplification parameter. Parameters S, T_B, T_C, T_D and β depend on soil class and on the level of seismicity (Type 1 or Type 2), following the EC8 scheme.

Table 4. Proposed Soil and Site Characterization.

Soil Class	Description	T_0 (s)	Remarks
A1	Rock formations		$V_s \geq 1500$m/s
A2	Slightly weathered / segmented rock formations (thickness of weathered layer <5.0m)	≤0.2	Surface weathered layer: $V_{s,av} \geq 200$m/s Rock Formations: $V_s \geq 800$m/s
	Geologic formations resembling rock formations in their mechanical properties and their composition (e.g. conglomerates)		$V_s \geq 800$m/s
B1	Highly weathered rock formations whose weathered layer has a considerable thickness (5m - 30m)	≤0.5	Weathered layer: $V_{s,av} \geq 300$m/s
	Soft rock formations of great thickness or formations which resemble these in their mechanical properties (e.g. stiff marls)		$V_{s,av}$: 400-800m/s $N_{SPT} > 50$, Su> 200kPa
	Soil formations of very dense sand – sand gravel and/or very stiff/ to hard clay, of homogenous nature and small thickness (up to 30m)		$V_{s,av}$: 400-800m/s $N_{SPT} > 50$, $S_u > 200$kPa
B2	Soil formations of very dense sand – sand gravel and/or very stiff/ to hard clay, of homogenous nature and medium thickness (30-60m), whose mechanical properties increase with depth	≤0.8	$V_{s,av}$: 400-800m/s $N_{SPT} > 50$, $S_u > 200$kPa
C1	Soil formations of dense to very dense sand – sand gravel and/or stiff to very stiff clay, of great thickness (>60m), whose mechanical properties and strength are constant and/or increase with depth	≤1.5	$V_{s,av}$: 400-800m/s $N_{SPT} > 50$, $S_u > 200$kPa
C2	Soil formations of medium dense sand – sand gravel and/or medium stiffness clay (PI > 15, fines percentage > 30%) of medium thickness (20–60m)	≤1.5	$V_{s,av}$: 200-450m/s $N_{SPT} > 20$, $S_u > 70$kPa
C3	Category C2 soil formations of great thickness (>60m), homogenous or stratified that are not interrupted by any other soil formation with a thickness of more than 5.0m and of lower strength and $V_{s,av}$ velocity	≤1.8	$V_{s,av}$:200-450m/s $N_{SPT} > 20$, $S_u > 70$kPa
D1	Recent soil deposits of substantial thickness (up to 60m), with the prevailing formations being soft clays of high plasticity index (PI>40), high water content and low values of strength parameters	≤2.0	$V_{s,av} \leq 300$m/s $N_{SPT} < 25$, $S_u < 70$kPa
D2	Recent soil deposits of substantial thickness (up to 60m), with prevailing fairly loose sandy to sandy-silty formations with a substantial fines percentage (not to be considered susceptible to liquefaction)	≤2.0	$V_{s,av} \leq 300$m/s $N_{SPT} < 25$
D3	Soil formations of great overall thickness (>60m), interrupted by layers of category D1 or D2 soils of a small thickness (5.0 – 15.0m), up to the depth of ~40m, within soils (sandy and/or clayey, category C) of evidently greater strength, with $V_{s,av} \geq 300$m/s	≤3.0	$V_{s,av}$: 150-600m/s
E	Surface soil formations of small thickness (5–20m), small strength and stiffness, likely to be classified as category C and D according to its geotechnical properties, which overlie category A formations ($V_{s,av} \geq 800$m/s)	≤0.7	Surface soil layers: $V_{s,av} \leq 400$m/s
X	Loose fine sandy-silty soils beneath the water table, susceptible to liquefaction (unless a special study proves no such danger, or if the soil's mechanical properties are improved), Soils near obvious tectonic faults, Steep slopes covered with loose lateral deposits, Loose granular or soft silty-clayey soils, provided they have been proven to be hazardous in terms of dynamic compaction or loss of strength. Recent loose landfills, Soils with a very high percentage in organic material, Soils requiring site-specific evaluations.		

To determine parameters T_B, T_C, T_D and β, which define the shape of the response spectra, subset DS4 of the SHARE-AUTH database was used. The normalized acceleration response spectra from the selected strong-motion records, i.e. the acceleration spectra divided by PGA, were plotted for each soil class and for the two levels of seismicity. For each soil class and level of seismicity, the median normalized acceleration spectra, as well as the 16th and 84th percentiles were calculated. The proposed normalized acceleration response spectra were evaluated through fitting the general spectral equations as close as possible to the 84th percentile, in order to account for the uncertainties associated with the nature of the problem. Moreover, it was considered important that the same degree of conservatism was followed for all soil classes, and spectral periods, which is not the case for the normalized response spectra of EC8 (Pitilakis et al. 2012). The plots illustrating the median and the range between 16th and 84th percentiles, and the proposed design normalized acceleration spectra for all the new soil classes are available in Pitilakis et al. (2013). Type 2 spectra generally exhibit a narrower range of constant spectral acceleration compared to Type 1. This justifies the decision to select two different spectrum types, since, in this way, overestimation of spectral ordinates in areas affected only by low-to-moderate magnitude earthquakes can be avoided.

Soil amplification factors S for the proposed classification system were estimated using the logic tree approach described earlier using dataset DS4. Table 5 summarizes the soil amplification factors obtained for all soil classes with the two different approaches, as well as the weighted average and proposed S values. For soil classes B1, B2, C1, C2 and C3, the new soil amplification factors resulted from rounding the weighted average of the soil factors estimated with Approaches 1 and 2. For soil class D, where actually limited data are available, we slightly reduced the soil amplification factors calculated from the logic tree approach, since we judged them as over-conservative. In contrast, for soil class E, again due to the relatively small dataset, we decided to maintain the soil factor values proposed by EC8, since the definition of soil classes E in EC8 and the new classification system are similar. Site-specific ground response analyses for both soil classes D and E should be recommended by the seismic code provisions.

The proposed coefficients T_B, T_C, T_D, β and S defining the elastic response spectra for the new soil classes are given in Table 6. The proposed elastic acceleration response spectra, normalized to the design ground acceleration at rock-site conditions PGA_{rock}, are illustrated in Figure 3.

Table 5. Soil factors for the new classification system.

Soil Class	**Type 2 (M_s≤5.5)**				**Type 1 (M_s>5.5)**			
	Approach 1	Approach 2	Weighted Average	Proposed	Approach 1	Approach 2	Weighted Average	Proposed
B1	1.28	0.99	1.13	1.20	1.03	1.03	1.03	1.10
B2	1.89	1.17	1.53	1.50	1.36	1.28	1.32	1.30
C1	2.02	1.46	1.74	1.80	2.19	1.27	1.73	1.70
C2	2.08	1.39	1.74	1.70	1.35	1.15	1.25	1.30
C3	2.59	1.61	2.10	2.10	1.57	1.07	1.32	1.30
D	2.19	2.26	2.23	2.00[a]	2.03	1.79	1.91	1.80[a]
E	1.54	1.30	1.42	1.60[a]	1.10	0.94	1.02	1.40[a]

(a) site specific ground response analysis required

Table 6. Parameters of the proposed acceleration response spectra.

Soil Class	Type 2 ($M_s \leq 5.5$)					Type 1 ($M_s > 5.5$)				
	T_B (s)	T_C (s)	T_D (s)	S	β	T_B (s)	T_C (s)	T_D (s)	S	β
A	0.05	0.30	1.2	1.0	2.5	0.10	0.40	2	1.0	2.5
B1	0.05	0.25	1.2	1.2	2.75	0.10	0.40	2	1.1	2.75
B2	0.05	0.30	1.2	1.5	2.5	0.10	0.50	2	1.3	2.5
C1	0.10	0.25	1.2	1.8	2.5	0.10	0.60	2	1.7	2.5
C2	0.10	0.40	1.2	1.7	2.5	0.10	0.60	2	1.3	2.5
C3	0.10	0.50	1.2	2.1	2.5	0.10	0.90	2	1.3	2.5
D[a]	0.10	0.70	1.2	2.0	2.5	0.10	0.70	2	1.8	2.5
E[a]	0.05	0.20	1.2	1.6	2.75	0.10	0.35	2	1.4	2.75
(a) site specific ground response analysis required										

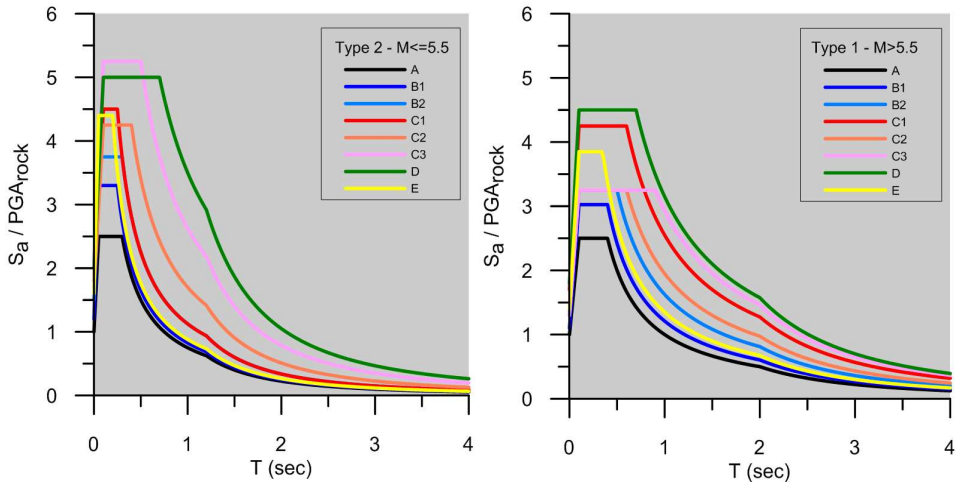

Figure 3. Type 2 (left) and Type 1 (right) elastic acceleration response spectra for the proposed classification system.

Amplification factors for complex subsurface geometry

Description of the parametric analyses

The parametric analyses include a total of 96 trapezoidal basin models. For all the models, linear viscoelastic analyses for 10 different input motions were performed using the finite difference 2DFD_DVS code (Moczo et al., 2007, Moczo et al., 2004, Kristek and Moczo, 2003). Makra et al. (2012) in a previous parametric study verified the efficiency of this code in reproducing complex seismic wavefields in idealized 2D basins. In the present study 32 geometries, described by their width, w, depth, h and sloping edge angles, a1-a2 (Figure 4), were studied, which correspond to four h/0.5w shape ratios (see Table inside Figure 4) and four sets of a1-a2 angle combinations (20^o-20^o, 45^o-45^o, 65^o-65^o, 20^o-65^o). For each geometrical configuration three different materials were considered for the sediments (Table 7), resulting to a total of 96 models. The 96 models were analyzed for one Gabor pulse and nine accelerograms selected from the

SHARE strong motion database (Yenier et al., 2010) to have been recorded at EC8 soil class A (rock) sites. The selected accelerograms originate from earthquakes with magnitude M_w ranging between 5.3 and 7.6, different types of faulting systems and epicentral distances, to form a set of input motions with variable frequency content and duration due to fault and path effects. A total number of 960 analyses were performed. Each analysis is assigned with a code ID $w_i h_j a_k Vs_l in_m$ indicating different combinations of widths (w_i), thicknesses (h_j), angles sets (a_k), sediments materials (Vs_l) and input motions (in_m) according to Table 8.

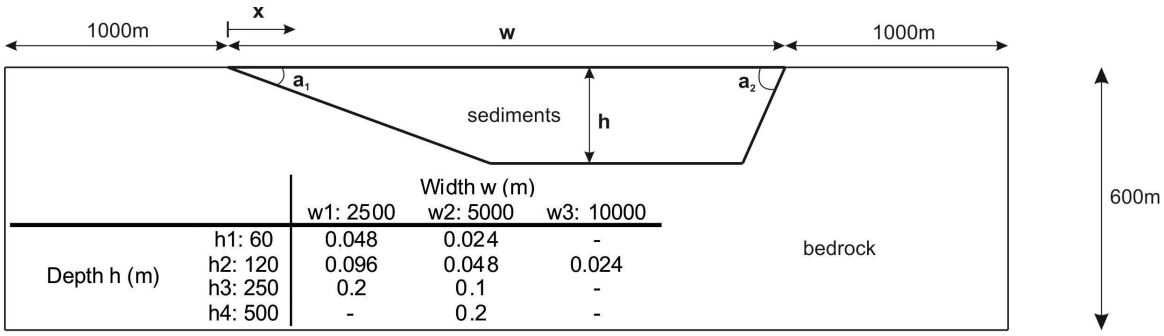

Figure 4. Geometrical properties of the studied basins.

Table 7. Material properties of basin sediments and bedrock.

	Material property	Material 1	Material 2	Material 3
Sediments	S-wave velocity (V_s in m/s)	250	350	500
	Quality factor of S-waves (Q_s)*	25	35	50
	P-wave velocity (V_p in m/s)	1600	1750	2000
	Quality factor of P-waves (Q_p)*	50	70	100
	Density (ρ in kg/m^3)	2000		
Bedrock	S-wave velocity (V_s in m/s)	1500		
	Quality factor of S-waves (Q_s)*	∞		
	P-wave velocity (V_p in m/s)	3000		
	Quality factor of P-waves (Q_p)*	∞		
	Density (ρ in kg/m^3)	2500		

* Quality factor Q: a non-dimensional factor expressing damping ξ ($Q=1/2\xi$). For the sediments the equations $Q_s=V_s/10$ and $Q_p=2Q_s$ were used.

Table 8. Nomenclature of the analyzed models.

i,j,k,l,m	**w_i**	**h_j**	**a_k**	**Vs_l**	**in_m**
1	2500m	60m	$a_1=a_2=20^o$	material 1	Gabor
2	5000m	120m	$a_1=a_2=45^o$	material 2	input2
3	10000m	250m	$a_1=a_2=65^o$	material 3	input3
4	-	500m	$a_1=20^o$, $a_2=65^o$	-	input4
5-10	-	-	-	-	input5-10

Aggravation factors

To estimate the additional effect of the 2D response at different locations at the surface of the basin with respect to the corresponding 1D response of the isolated soil columns in each location, period-dependent seismic aggravation factors (AGF) were computed (equation 8), defined as the ratio between 2D and corresponding 1D acceleration response spectra at the basin surface (Chávez-García and Faccioli, 2000). For each model and input motion in_m (m=2,10), the acceleration time histories from the 2D and 1D numerical simulations were used to estimate the 5% damped acceleration response spectra $SA_{m,2D}(T)$ and $SA_{m,1D}(T)$ respectively at each location and then the period-dependent aggravation factors with equation 8:

$$AGF_m(T) = \frac{SA_{m,2D}(T)}{SA_{m,1D}(T)} \tag{8}$$

Then, a mean period-dependent aggravation factor $\overline{AGF}(T)$ at each location at the surface of the basin was considered (equation 9) for input motions in_m (m=2,10):

$$\overline{AGF}(T) = \frac{\sum_{m=2}^{10} AGF_m(T)}{9} \tag{9}$$

Figure 5a illustrates indicatively the period-dependent aggravation factors $AGF_i(T)$ at the center of model w1h2a2Vs2 for input motions in2-in10, as well as the mean aggravation factor $\overline{AGF}(T)$ at the same site.

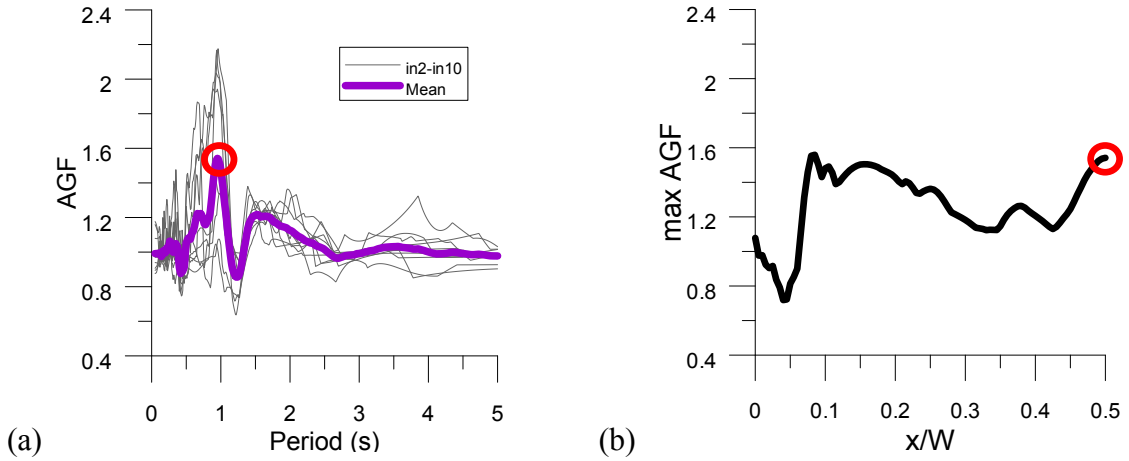

Figure 5. Model w1h2a2Vs2: (a) Period-dependent aggravation factors for input motions in2-in10 and mean period-dependent aggravation factor for the receiver located in the center, (b) Spatial distribution of the maximum aggravation factors along the half-width of the model.

In order to identify the maximum amplification of ground motion that can be attributed to the 2D response of the basin, the maximum values of the mean aggravation factors were selected along the surface of each model, regardless of the spectral period of their occurrence. In Figure 5a, the

red circle illustrates the maximum aggravation factor for the receiver located at the centre of model (x/w=0.5). The spatial distribution of the maximum aggravation factors for all receivers along the half-width of the symmetrical model is illustrated in Figure 5b. In general it is observed that maximum aggravations for the majority of the models appear at spectral periods around or somewhat lower than the resonant period of each model.

Figure 6 shows some indicative results of the effect of depth h (Figures 6a, 6b), width w (Figure 6c) and inclination angles (Figure 6d) on the maximum AGF for symmetrical basins. In general the increase of depth leads to an increase of maximum AGF, especially for sediments with low V_s value. The increase is more pronounced close to the centre of the basin (Figures 6a and 6b). The increase of the width of the basin leads to smaller maximum AGF as we move towards the centre of the basin (e.g. Figure 6c). This can be attributed to the attenuation with distance of locally generated at the edges surface waves, which, for the case of the wider configurations, results to an almost 1D response at the centre of the basin. Variation in inclination angle affects only the region above the basin edge, where maximum aggravation factors less than unity appear for steep angles (e.g. Figure 6d), meaning that ground motion is deamplified compared to the 1D estimation. This may be due to the fact that for 1D analyses, the total amount of the incoming seismic energy is trapped within the sedimentary layer, leading to amplification due to 1D resonance, while in 2D analyses part of the energy is diffracted at the lateral sides and generates surface waves. Non-symmetrical basins behave in a way similar to the corresponding symmetrical models.

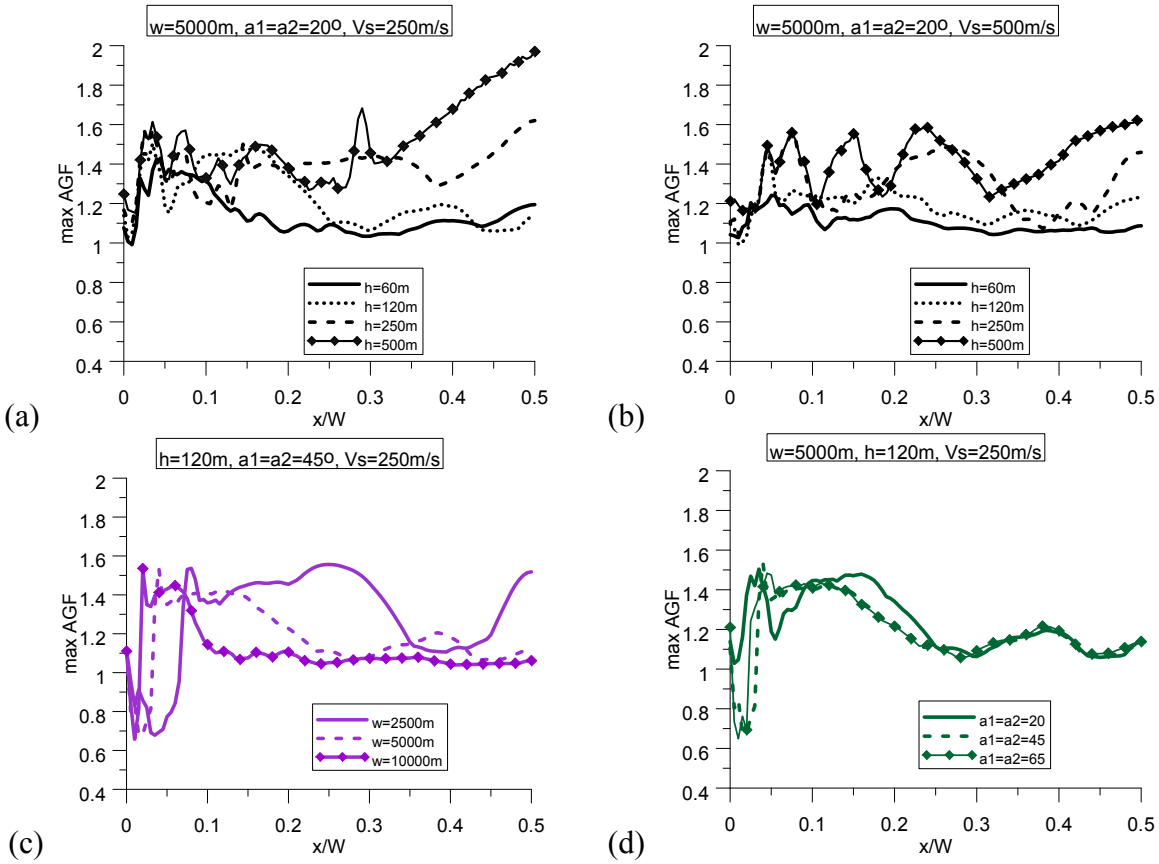

Figure 6. Maximum aggravation factor along the surface of the basin.

Since we are mainly interested in deriving practical recommendations for ordinary engineering applications, it is obligatory to propose median values instead of the maximum ones. For this reason the basin was divided into regions, and the mean aggravation factors $\overline{AGF}(T)$ were averaged over the locations belonging to each region. For the symmetrical basins, the half-width of the basin was divided into five regions (a_1, b_1, c_1, d_1 and e_1) with two equal-width regions (a_1 and b_1) over the inclined part of the basin-bedrock discontinuity and three equal-width regions (c_1, d_1 and e_1) over the constant-depth part of the basin (Figure 7a). For the non-symmetrical basins, five additional regions were applied to the second half-width of the basin (Figure 7a). Figure 7b illustrates the results for the symmetrical basin with width w=5000m, depth h=250m, inclination angles $a_1=a_2=20^o$ and shear wave velocity of the sediments V_s=250m/s. Aggravation factors are plotted versus the period normalized to the fundamental period at the center of the basin T_0, around which maximum aggravation for the constant-depth part of the basin occurs. The maximum values for the average AGF per region can be found in Pitilakis et al. (2014).

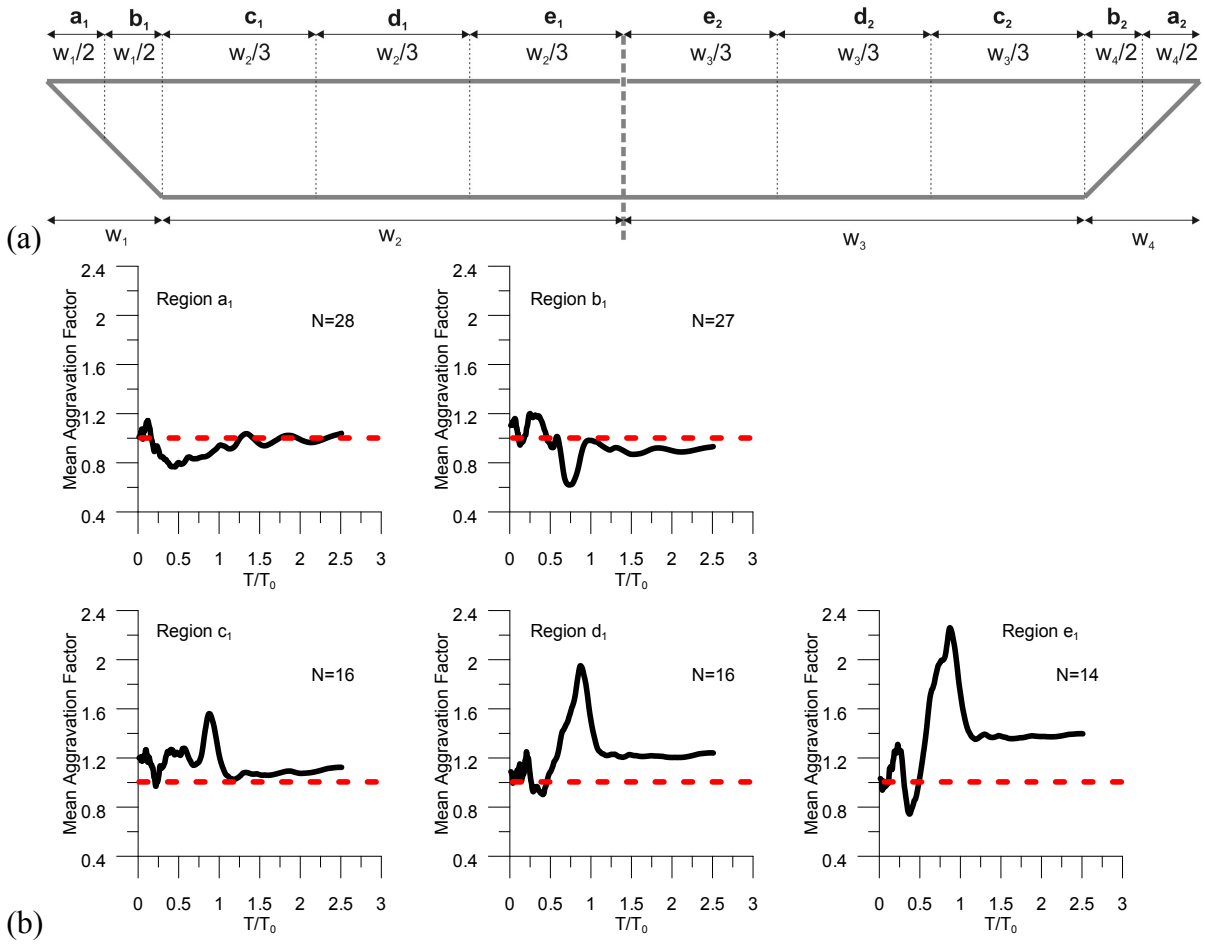

Figure 7. (a) Division of basins into regions. For the symmetrical basins only regions a_1-e_1 are considered. (b) Aggravation factors for regions a_1, b_1, c_1, d_1, e_1 for model w1h3a1Vs1.

The results indicate that for the shallow and medium-thickness basins (i.e. with depths equal to 60m or 120m), the maximum aggravation factors appear at regions c_1 and d_1 for the symmetrical basins while for the non-symmetrical ones they systematically appear at region c1 (closer to the

left inclined boundary of 20º slope – the smallest between the two) with values ranging between 1.1 and 1.5 for both cases. For the deep basins (i.e. with depths equal to 250m or 500m), maximum values appear at regions a1 and e1 for the symmetrical models and mostly at regions e_2 and a_2 for the non-symmetrical ones and range between 1.4 and 2.8.

Finally, in order to take into consideration the period-dependency of aggravation factors, a short-period and a long-period average of the mean aggravation factors $\overline{AGF}(T)$ was determined. A visual inspection of the computed aggravation factors (e.g. Figure 8, which summarizes the AGF for all symmetrical models for three distinct periods $T=T_0$, $0.6T_0$ and $0.3T_0$, where T_0 is the fundamental period at the centre of the basin) led us to the conclusion that the results do not differentiate substantially for periods less than $0.75T_0$. Consequently, we calculated the short-period AGF_S by averaging the mean aggravation factors $\overline{AGF}(T)$ over periods less than $0.75T_0$, while the long-period AGF_L by averaging over the periods between $0.75T_0$ and $1.5T_0$. The median, 16th- and 84th-percentile values can be found in Pitilakis et al. (2014).

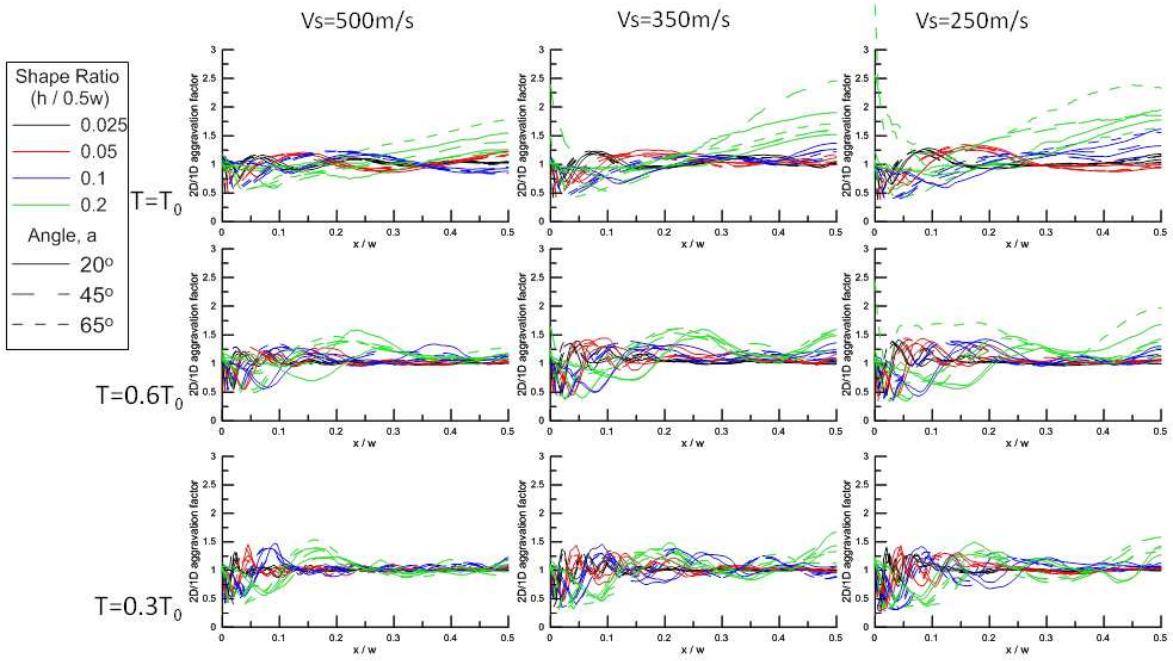

Figure 8. Aggravation factors for all symmetrical models for three distinct periods $T=T_0$, $0.6T_0$ and $0.3T_0$, where T_0 is the fundamental period at the centre of the basin.

Both AGF_S and AGF_L are in general less than unity above the inclined part of the basin (regions a_1 and b_1), which means that 1D response is higher than 2D response and decrease with increasing inclination angle. At the constant-depth part of the basin the median values for the short-period aggravation factor are quite low (around 1.10) with a quite narrow band between the 16th and 84th percentiles and do not vary substantially with inclination angle or sediments shear wave velocity (e.g. Figure 9a for region e_1). Figures 10a and 10b illustrate the dependence of the median and 16th- and 84th-percentile values of AGF_L on the sediments shear wave velocity and on the shape ratio of the basin (h/0.5w), respectively. At the constant-depth part of the basin (regions c_1, d_1 and e_1) median AGF_L are about 1.10 and converge to 1.00 for V_s=500m/s. The 84th percentiles, however, are strongly influenced by sediments V_s and can be as high as 1.70 for

region e_1 and V_s=250m/s (Figure 10a). Regarding the dependence of AGF_L on the shape ratio, we observe that in regions c_1, d_1 and e_1 AGF_L increase with increasing shape ratios, with median values lying between 1.10 and 1.40 and 84th percentiles as high as 1.80 for the highest shape ratio (Figure 9b). AGF_Lat the constant-depth part of the basin is also strongly affected by the fundamental period of the basin; basins with high T_0 exhibit much higher median AGF_L, as well as a wider band between the 16th and 84th percentiles, compared to basins with low T_0 (e.g. Figure 9b for region e_1).

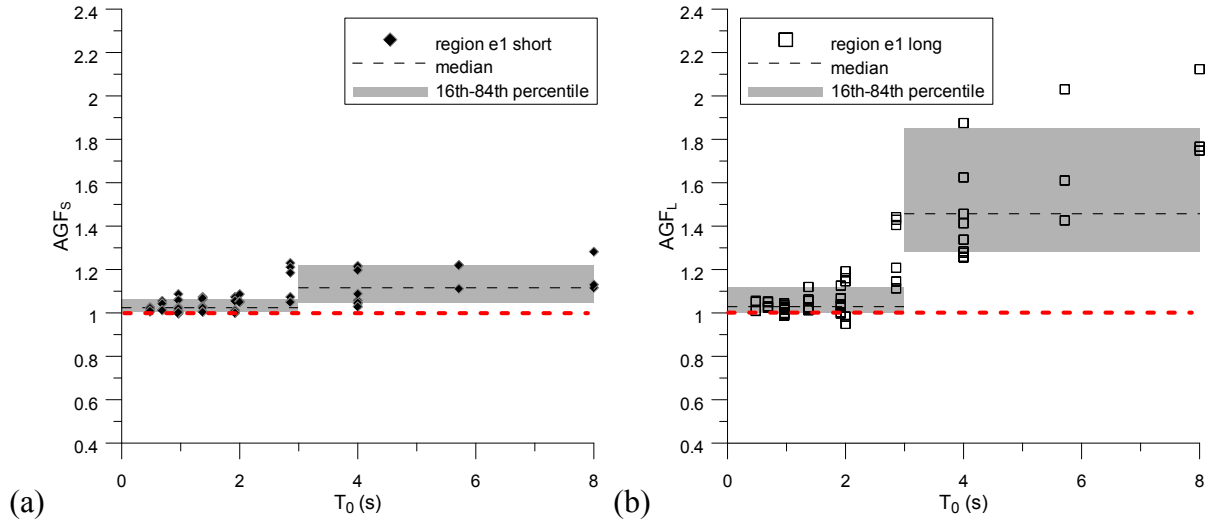

Figure 9. Influence of fundamental period at the center of the basin on (a) short-period aggravation factor AGF_S and (b) long-period aggravation factor AGF_L, at region e_1: Median, 16th- and 84th-percentile values.

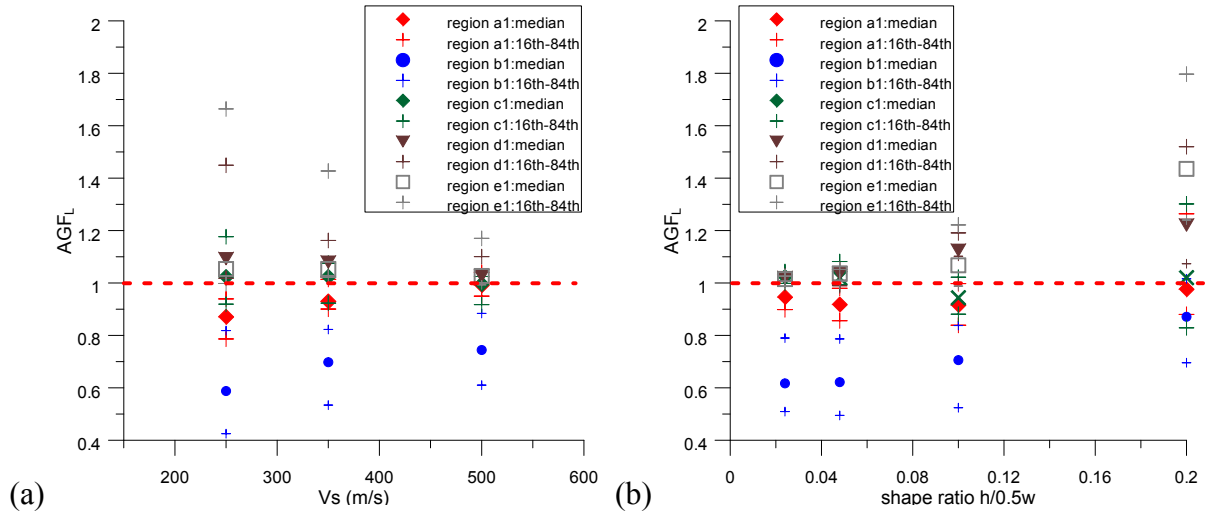

Figure 10. Influence of (a) shear wave velocity of sediments and (b) shape ratio, on long-period aggravation factor AGF_L: Median, 16th- and 84th-percentile values for all regions.

Preliminary proposals for EC8

Based on the above thorough parametric analysis it is believed that we have convincing arguments to propose, in case of normal shaped basins of trapezoidal shape, a short-period aggravation factor AGF_S ($T \leq 0.75T_0$) and a long-period aggravation factor AGF_L ($T > 0.75T_0$) for the seismic design of structures with fundamental vibration periods T falling within these period bands (T_0 is the fundamental period at the center of the basin). The proposed aggravation factor should multiply in each period range the spectral value of the design elastic response spectrum of EC8. Spatial distribution of AGF_S and AGF_L along the basin showed that for the region above the inclined part of the basin, both AGF_S and AGF_L are in general below 1.0, thus, in order to be on the safe side, the design response spectrum (i.e. normally the seismic code values) can be used without any further modification for basin edge effects. On the contrary, for the region above the constant-depth part of the basin, median short-period aggravation factors AGF_S are around 1.1 with 84^{th} percentiles not greater than 1.2; median long-period aggravation factors AGF_L are around 1.0 for basins with low T_0, while vary from 1.1 to 1.4 for basins with higher T_0. Corresponding AGF_L 84^{th} percentiles are 1.1 for low-T_0 basins and can be as high as 1.8 for high-T_0 basins. The limit value of T_0 for the distinction between low- and high-T_0 basins could be indicatively set to 3.0s (Figure 9). These aggravation factors should be mainly used for ordinary structures, while detailed site-specific analyses should be performed for important structures.

Conclusions

The aim of the present work is to provide recommendations for the improvement of EC8 in terms of site effects with the predominance of 1D ground response and in a second stage to account for complex 2D site effects related to the existence of subsurface geometry usually referred as basin effects. To this end, a large worldwide dataset of strong motion records was used to propose improved soil amplification factors for the current classification scheme of EC8, as well as a new improved soil and site classification system with the accompanying elastic response spectra. The new soil-site classification system uses parameters such as the thickness of soil deposits above the seismic bedrock (V_s>800m/s), the average shear wave velocity to the seismic bedrock and the fundamental period of the site; it is believed that it is more precise, convenient and practical from a geotechnical engineering point of view. Extensive parametric 2D numerical analyses of the seismic response of homogeneous alluvial basins were performed at a second stage to explore the basin-induced amplification and its sensitivity to parameters related to the basin geometry and the properties of the soil sediments. The computed maximum AGF were found as high as 2.8 for some specific geometries and soil conditions. Median and 84^{th} percentiles values are proposed for ordinary engineering applications with the introduction of a short- (for periods $T \leq 0.75T_0$, where T_0 is the fundamental period at the center of the basin) and a long-spectral period ($T > 0.75T_0$) aggravation factor, which should multiply the present spectral value of the elastic response spectrum in order to account for the extra amplification in case of basins. The extra median factors vary from 1.0 to 1.4 with the largest values corresponding to the deeper basins, with corresponding 84^{th} percentiles ranging from 1.1 to 1.8.

Acknowledgments

This research has been funded by the European Community's Seventh Framework Program [FP7/2007–2013] under grant agreements no 226967 (SHARE) and 262330 (NERA), as well as

the General Secretariat for Research and Technology, under contract no. 11ΣΥΝ_8_1577 (Development of Earthquake Rapid Response System for Metropolitan Motorways).

References

Akkar S, Bommer JJ. Empirical equations for the prediction of PGA, PGV and spectral accelerations in Europe, the Mediterranean region and the Middle East. *Seismological Research Letters* 2010; **81** (2): 195-206.

Bard PY, Bouchon M. The seismic response of sediment-filled valleys. Part 1. The case of incident SH waves. *Bulletin of the Seismological Society of America* 1980a; **70** (4): 1263–1286.

Bard PY, Bouchon M. The seismic response of sediment-filled valleys. Part 2. The case of incident P and SV waves. *Bulletin of the Seismological Society of America* 1980b; **70** (5): 1921–1941.

Bard PY, Bouchon M. The two-dimensional resonance of sediment-filled valleys. *Bulletin of the Seismological Society of America* 1985; **75** (2): 519-541.

Bielak J, Xu J, Ghattas O. Earthquake ground motion and structural response in alluvial valleys. *Journal of Geotechnical and Geoenvironmental Engineering* 1988; **125** (5), 413–423.

Borcherdt RD, Glassmoyer G. On the characteristics of local geology and their influence on ground motions generated by the Loma Prieta earthquake in the San Francisco bay region, California. *Bulletin of the Seismological Society of America* 1992; **82** (2): 603–641.

Bray JD, Rodríguez-Marek A. Geotechnical site categories. *In Proc. of the First PEER-PG&E Workshop on Seismic Reliability of Utility Lifelines*. San Francisco, California, USA, 1997.

Cadet H, Bard PY, Rodriguez-Marek A. Site effect assessment using KiK-net data: Part 2 - site amplification prediction equation based on f_0 and V_{sz}. *Bulletin of Earthquake Engineering* 2012; **10** (2): 451-489.

Castellaro S, Mulargia F, Rossi PL. Vs30: proxy for seismic amplification? *Seismological Research Letters* 2008; **79** (4):540–543.

Cauzzi C, Faccioli E. Broadband (0.05 to 20 s) prediction of displacement response spectra based on worldwide digital records. *Journal of Seismology* 2008; **12** (4): 453–475.

CEN (European Committee for Standardization). *Eurocode 8: Design of structures for earthquake resistance, Part 1: General rules, seismic actions and rules for buildings*. EN 1998-1:2004. Brussels, Belgium, 2004.

Chávez-García FJ, Faccioli E. Complex site effects and building codes: Making the leap. *Journal of Seismology* 2000; **4** (1): 23–40.

Chiou BSJ, Youngs RR. An NGA model for the average horizontal component of peak ground motion and response spectra. *Earthquake Spectra* 2008; **24** (1): 173–215.

Choi Y, Stewart JP. Nonlinear site amplification as function of 30 m shear wave velocity. *Earthquake Spectra* 2005; **21** (1): 1-30.

Delavaud E, Cotton F, Akkar S, Scherbaum F, Danciu L, Beauval C, Drouet S, Douglas J, Basili R, Sandikkaya MA, Segou M, Faccioli E, Theodoulidis N. Toward a ground-motion logic tree for probabilistic seismic hazard assessment in Europe. *Journal of Seismology* 2012; **16** (3): 451-473.

Gallipoli MR, Mucciarelli M. Comparison of site classification from V*S30*, V*S10*, and HVSR in Italy. *Bulletin of the Seismological Society of America* 2009; **99** (1): 340-351.

Graves RW. Modeling three-dimensional site response effects in the Marina district basin, San Francisco, California. *Bulletin of the Seismological Society of America* 1993; **83** (4): 1042–1063.

Housner GW. *Spectrum intensities of strong-motion earthquakes. In Proc. of the symposium on earthquakes and blast effects on structures*. Earthquake Engineering Research Institute, 1952.

Japan Road Association. *Specifications for Highway Bridges Part V*. Seismic Design,Maruzen Co., LTD, 1980.

Kawase H. The Cause of the Damage Belt in Kobe: "The Basin-Edge Effect," Constructive Interference of the

Direct S-Wave with the Basin-Induced Diffracted/Rayleigh Waves. *Seismological Research Letters* 1996; **67** (5): 25–34.

Kristek J, Moczo P. Seismic wave propagation in viscoelastic media with material discontinuities – a 3D 4th-order staggered-grid finite-difference modeling. *Bulletin of the Seismological Society of America* 2003; **93** (5): 2273-2280.

Lee VW, Trifunac MD. Should average shear-wave velocity in the top 30m of soil be used to describe seismic amplification? *Soil Dynamics and Earthquake Engineering* 2010; **30** (11): 1250-1258.

Luzi L, Puglia R, Pacor F, Gallipoli MR, Bindi D, Mucciarelli M. Proposal for a soil classification based on parameters alternative or complementary to $V_{s,30}$. *Bulletin of Earthquake Engineering* 2011; **9** (6): 1877–1898.

Makra K, Gelagoti F, Ktenidou OJ, Pitilakis K. basin effects in seismic design: Efficiency of numerical tools in reproducing complex seismic wavefields. In *Proc. of 12th World Conference on Earthquake Engineering*, 2012.

Moczo P, Kristek J, Galis M, Pazak P, Balazovjech M. The Finite Difference and Finite- Element Modeling of Seismic Wave Propagation and Earthquake Motion. *Acta Physica Slovaca* 2007; **57** (2): 177- 406.

Moczo P, Kristek J, Galis M. Simulation of planar free surface with near-surface lateral discontinuities in the finite-difference modeling of seismic motion. *Bulletin of the Seismological Society of America* 2004; **94** (2): 760-768.

Papageorgiou AS, Kim J. Study of the propagation and amplification of seismic waves in Caracas valley with reference to the 29 July 1967 earthquake: SH waves. *Bulletin of the Seismological Society of America* 1991; **81** (6): 2214–2233.

Pitilakis K. Site effects. In Ansal A (ed) *Recent advances in earthquake geotechnical engineering and microzonation,* pp 139-197, Kluwer Academic Publishers, 2004.

Pitilakis K, Gazepis C, Anastasiadis A. Design response spectra and soil classification for seismic code provisions. In *Proc. of 13th World Conference on Earthquake Engineering,* paper n. 2904, Vancouver, Canada, 2004

Pitilakis K, Riga E, Anastasiadis A. Design spectra and amplification factors for Eurocode 8. *Bulletin of Earthquake Engineering* 2012; **10** (5): 1377-1400.

Pitilakis K, Riga E, Anastasiadis A. New code site classification, amplification factors and normalized response spectra based on a worldwide ground-motion database. *Bulletin of Earthquake Engineering* 2013; **11** (4): 925–966.

Pitilakis K, Riga E, Makra K, Gelagoti F, Ktenidou O-J, Anastasiadis A, Pitilakis D, Izquierdo Flores CA. Deliverable D11.5, Code cross-check, computed models and list of available results - AUTH contribution, *NERA: Network of European Research Infrastructures for Earthquake Risk Assessment and Mitigation*, 2014.

Rey J, Faccioli E, Bommer JJ. Derivation of design soil coefficients (S) and response spectral shapes for Eurocode 8 using the European Strong-Motion Database. *Journal of Seismology* 2002; **6** (4): 547-555.

Sánchez-Sesma FJ, Perez-Rocha LE, Chávez-Pérez S. Diffraction of elastic waves by three-dimensional surface irregularities. Part II. *Bulletin of the Seismological Society of America* 1989; **79** (1): 101–112.

Trifunac MD. Surface motion of a semi-cylindrical alluvial valley for incident plane SH waves. *Bulletin of the Seismological Society of America* 1971; **61** (6): 1755–1770.

Steidl JH. Site response in southern California for probabilistic seismic hazard analysis. *Bulletin of the Seismological Society of America* 2000; **90** (6B): S149–S169.

Wong HL, Trifunac MD. Surface motion of a semi-elliptical alluvial valley for incident plane SH waves. *Bulletin of the Seismological Society of America* 1974; **64**(5): 1389–1408.

Yegian MK, Ghahraman VG, Gazetas G. Seismological, soil and valley effects in Kirovakan, 1988 Armenia earthquake. *Journal of Geotechnical Engineering* 1994; **120** (2): 349–365.

Yenier E, Sandikkaya MA, Akkar S. Report on the fundamental features of the extended strong motion databank prepared for the SHARE project (v1.0), 2010.

Zhao JX, Zhang J, Asano A, Ohno Y, Oouchi T, Takahashi T, Ogawa H, Irikura K, Thio HK, Somerville PG, Fukushima Y, Fukushima Y. Attenuation relations of strong ground motion in Japan using site classification based on predominant period. *Bulletin of the Seismological Society of America* 2006; **96** (3): 898–913.